

# Role of DNA binding sites and slow unbinding kinetics in titration-based oscillators

Sargis Karapetyan<sup>1,2</sup> and Nicolas E. Buchler<sup>1,2,3</sup>

<sup>1</sup>*Department of Physics, Duke University, Durham, NC 27708*

<sup>2</sup>*Center for Genomic & Computational Biology, Durham, NC 27710*

<sup>3</sup>*Department of Biology, Duke University, Durham, NC 27708*

(Dated: March 9, 2022)

Genetic oscillators, such as circadian clocks, are constantly perturbed by molecular noise arising from the small number of molecules involved in gene regulation. One of the strongest sources of stochasticity is the binary noise that arises from the binding of a regulatory protein to a promoter in the chromosomal DNA. In this study, we focus on two minimal oscillators based on activator titration and repressor titration to understand the key parameters that are important for oscillations and for overcoming binary noise. We show that the rate of unbinding from the DNA, despite traditionally being considered a fast parameter, needs to be slow to broaden the space of oscillatory solutions. The addition of multiple, independent DNA binding sites further expands the oscillatory parameter space for the repressor-titration oscillator and lengthens the period of both oscillators. This effect is a combination of increased effective delay of the unbinding kinetics due to multiple binding sites and increased promoter ultrasensitivity that is specific for repression. We then use stochastic simulation to show that multiple binding sites increase the coherence of oscillations by mitigating the binary noise. Slow values of DNA unbinding rate are also effective in alleviating molecular noise due to the increased distance from the bifurcation point. Our work demonstrates how the number of DNA binding sites and slow unbinding kinetics, which are often omitted in biophysical models of gene circuits, can have a significant impact on the temporal and stochastic dynamics of genetic oscillators.

## I. INTRODUCTION

Genetic oscillatory networks are ubiquitous in nature and perform important functions. For example, the cell cycle oscillator regulates cell growth and division, whereas the circadian clock regulates the behavior of organisms with respect to daily changes in light. These genetic oscillators are used by living systems to reliably coordinate various periodic internal processes with each other as well as with their rhythmic environment. However, this presents a challenge at the cellular level because oscillators have to maintain proper timing (temporal coherence of oscillation) in the presence of stochastic noise that arises from the small number of regulatory molecules in cells [1].

A simple mechanism to mitigate the effect of molecu-

lar noise would be to increase the number of molecules of each species [2–4]. While the number of RNAs and proteins made per gene can be large, most cells are fundamentally constrained to 1-2 gene copies and are subject to binary noise in the first step of gene regulation (i.e., transcription factor binding to DNA) [5, 6]. This binary gene regulation noise manifests itself as a stochastic temporal pattern of all-or-none gene activity depending on whether the promoter is bound by the regulatory protein or not. Recent work shows that slow DNA binding/unbinding kinetics (also called the non-adiabatic limit) can exacerbate the binary noise and have profound consequences on gene expression [7], epigenetic switching [8], and oscillation [3, 4, 9, 10]. Faster kinetic rates and complex gene promoter architectures have been proposed as a way to suppress the effect of this binary noise. For example, increasing the DNA binding/unbinding rate can increase temporal coherence of oscillations via more precise sampling of the concentration of transcription factors [3, 9–11] or by increasing the distance from a bifurcation point [4, 12]. However, transcription factors often have slow DNA unbinding rates [13–17], which suggests that these mechanisms are not generally applicable. The cooperative binding of a transcription factor to multiple binding sites has also been shown to increase temporal coherence of oscillations [18]. However, multiple binding sites do not always lead to cooperativity and transcription factor binding to a single DNA site may often be enough to effectively activate or repress transcription.

To better understand the potential mechanisms that suppress the binary gene regulation noise, in particular the influence of slow DNA unbinding rates and multiple binding sites, we study an Activator-Titration Cir-

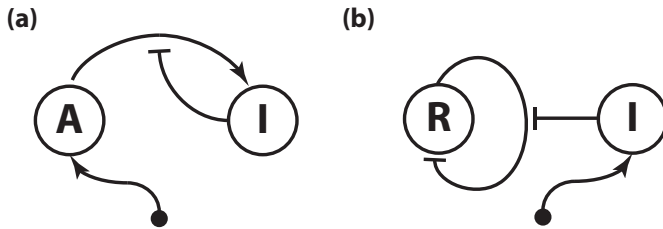


FIG. 1. (a) In the Activator-Titration Circuit (ATC), the activator is constitutively produced at a constant rate and activates the expression of the inhibitor, which, in turn, titrates the activator into inactive complex. (b) In the Repressor-Titration Circuit (RTC) the constitutively expressed inhibitor titrates the self-repressing repressor.

cuit (ATC) that has been theoretically shown to oscillate [19]. The ATC consists of a constitutively-expressed activator that promotes the expression of the inhibitor, which then titrates the activator into an inactive heterodimer complex (Fig. 1). Studying the ATC has two advantages. First, it lies at the core of animal circadian clocks [20] and oscillatory NF- $\kappa$ B signaling [21, 22] and has served as a model of natural genetic oscillators [10, 19, 23–26]. Second, the ATC generates the necessary nonlinearities through protein titration [27] and does not require cooperative binding of activator to the inhibitor promoter. Thus, by studying a titration-based oscillator, we can better explore the kinetic effects of multiple binding sites on coherence independently of the effects that might arise from cooperativity. To obtain general insights that are not specific to activation, we also study a Repressor-Titration Circuit (RTC), which consists of a self-repressor and a constitutively-expressed inhibitor (Fig. 1). This novel titration-based oscillator is analogous to the ATC but uses repression instead of activation for the transcriptional regulation.

We first characterize these oscillators and how they depend on several key parameters in Section II. We deliberately constrain ourselves to physiological parameters found in a simple eukaryote *S. cerevisiae*, commonly known as budding yeast. We show that, in addition to slow mRNA degradation, slow DNA unbinding rates of transcription factors are important for providing the necessary delay in the negative feedback loop for oscillatory solutions. Thus, both the DNA unbinding rate and mRNA degradation rate can set the period of oscillation. We then demonstrate that the addition of multiple, independent binding sites has nontrivial effects on the ATC and the RTC. While multiple binding sites lengthen the period of both oscillators due to an effective increase in the delay of negative feedback, they dramatically increase the oscillatory solution space of the RTC only. This is because multiple, independent binding sites generate ultrasensitivity (i.e. strong nonlinear response to changes in regulatory protein concentration) in repression-based promoters only, and thus only RTC can benefit from this effect. In section III, we use stochastic Gillespie simulations to understand the extent to which DNA unbinding rates and numbers of binding sites suppress the molecular noise in ATC and RTC oscillators. We show that multiple binding sites increase the temporal coherence of oscillations by alleviating the binary noise resulting from discrete gene states. We also show that slower values of DNA unbinding rates are best for coherent oscillations in simple titration-based oscillators. Last, we compare and contrast our results on temporal coherence with those of previous models of genetic oscillators in Section IV.

## II. BIOPHYSICAL MODEL OF ATC AND RTC

Oscillators require negative feedback with nonlinearity and time delays [28]. Mechanistically, negative feedback

on gene expression can occur transcriptionally via repressors [29–31] or post-transcriptionally via phosphorylation [32–34], degradation [32, 34, 35], or titration of activators into inactive complexes by inhibitors [10, 19, 23–26]. The ATC is a minimal two-gene circuit that can oscillate through the use of protein titration both as a source of nonlinearity and indirect negative feedback. In the first phase of oscillation, high levels of free activator homo-dimerize, bind the promoter, and overproduce inhibitor until all free activator has been titrated into inactive heterodimer. In the second phase of oscillation, the remaining activator will unbind from the inhibitor promoter and be sequestered by inhibitor, thus causing the promoter to return to low levels of expression of inhibitor. The levels of inhibitor will eventually decline to a point where free activator can re-accumulate and restart the cycle.

In the RTC, protein titration is used exclusively as a source of nonlinearity and the negative feedback is directly achieved through auto-repression. In the first phase of oscillation, high levels of free repressor will homo-dimerize, bind directly to its own promoter, and re-

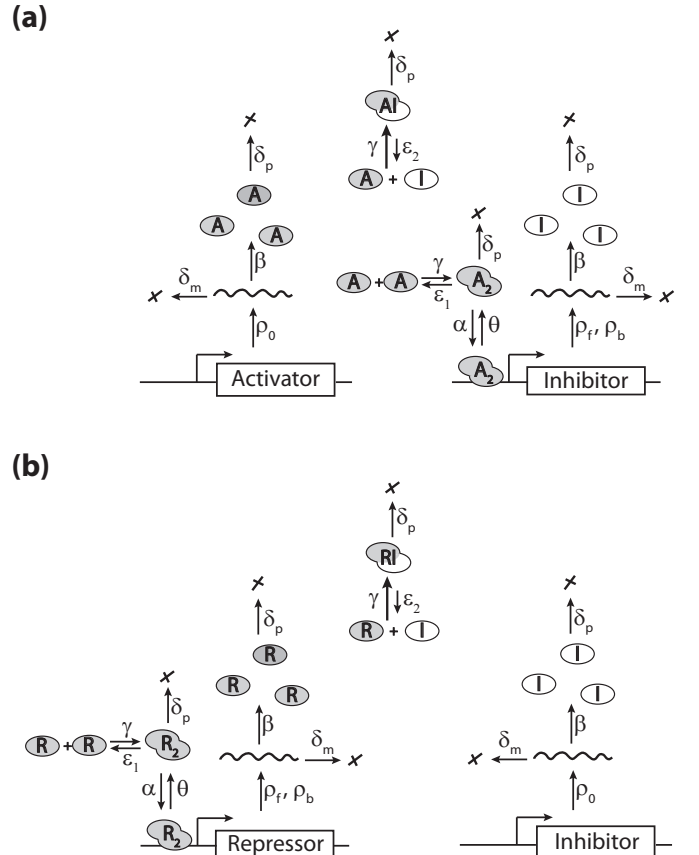


FIG. 2. A biophysical model for ATC (a) and RTC (b) with explicit transcription, translation, protein-protein and protein-DNA interactions. Each arrow corresponds to a reaction rate in Eqs. 1-3. Neither of these titration-based oscillators have been built or studied by synthetic biologists.

press its transcription. The free repressor will be titrated away by the constitutively expressed inhibitor. In the second phase of oscillation when free repressor levels are low, the remaining repressor will unbind from the promoter, returning to high levels of transcription and the rapid over-production of free repressor. As we will show below, the indirect versus direct nature of negative feedback in ATC and RTC is responsible for many of the differences between these two titration-based oscillators.

### A. ATC and RTC oscillators with a single DNA binding site

Even simple genetic circuits such as the ATC and RTC include many reactions and parameters (Fig. 2). An exhaustive search over all the parameter space was not feasible, and we decided to constrain our parameter space by studying synthetic gene circuits that could be built in budding yeast. Synthetic genetic oscillators have been useful tools to understand the properties of natural oscillators. For example, a synthetic oscillator built in bacteria [36] was useful in understanding entrainment capabilities

of genetic oscillators, as well as elucidating sources of stochasticity that affected entrainment. Surprisingly, all synthetic genetic oscillators built to date have neglected protein titration, a common mechanism in natural oscillators. To this end, we built a mathematical model of ATC and RTC oscillators using a basic leucine zipper (bZIP) transcription factor that dimerizes and binds DNA, and a rationally-designed inhibitor that binds free bZIP into an inactive heterodimer. These synthetic components have been successfully used in yeast [37] and, importantly, many of the protein-protein and protein-DNA binding affinities of this bZIP and inhibitor pair are known [38, 39]; see Table I. We fixed these parameters and scanned through a range of other biophysical parameters to understand which ones affect oscillation. Our results should help guide future experimental implementation of synthetic ATC and RTC oscillators in yeast.

The biophysical model of our ATC and RTC circuits is based on chemical mass-action kinetics where the dynamic variables are the mean concentrations of all molecular species. The ODEs that correspond to the reactions in Fig. 2 are the following:

$$\frac{d[G_0]}{dt} = -\alpha[G_0][X_2] + \theta[G_1] \quad (1a)$$

$$\frac{d[G_1]}{dt} = \alpha[G_0][X_2] - \theta[G_1] \quad (1b)$$

$$\frac{d[I]}{dt} = \beta[r_I] - \gamma[X][I] + \epsilon_2[XI] - \delta_p[I] \quad (1c)$$

$$\frac{d[X]}{dt} = \beta[r_X] - \gamma[X][I] + \epsilon_2[XI] - 2\gamma[X]^2 + 2\epsilon_1[X_2] - \delta_p[X] \quad (1d)$$

$$\frac{d[XI]}{dt} = \gamma[X][I] - \epsilon_2[XI] - \delta_p[XI] \quad (1e)$$

$$\frac{d[X_2]}{dt} = \gamma[X]^2 - \epsilon_1[X_2] - \delta_p[X_2] - \alpha[G_0][X_2] + \theta[G_1] \quad (1f)$$

With  $[r_X]$  and  $[r_I]$  described by:

$$\frac{d[r_X]}{dt} = \rho_0[G_T] - \delta_m[r_X] \quad (2a)$$

$$\frac{d[r_I]}{dt} = \rho_f[G_0] + \rho_b([G_T] - [G_0]) - \delta_m[r_I] \quad (2b)$$

for the ATC, where  $X=A$  (activator), and

$$\frac{d[r_X]}{dt} = \rho_f[G_0] + \rho_b([G_T] - [G_0]) - \delta_m[r_X] \quad (3a)$$

$$\frac{d[r_I]}{dt} = \rho_0[G_T] - \delta_m[r_I] \quad (3b)$$

for the RTC, where  $X=R$  (repressor). The first two equations represent the dynamics of promoter DNA

where  $[G_0]$  and  $[G_1]$  are the mean concentrations of free and bound promoter, respectively. The molar concentration of total DNA  $[G_T] = [G_0] + [G_1] = 1/(N_A \cdot V) = 1/24$  nM where  $N_A$  is the Avogadro constant and  $V$  is the yeast cell volume; see Table 1. Here, we consider only a single DNA binding site, but we will later expand our analysis to include multiple binding sites. At any instant, the promoter is either free or bound. The probability of free or bound promoters is equal to the ratio of concentrations  $[G_0]/[G_T]$  or  $[G_1]/[G_T]$ , respectively. The other equations describe the mean concentration dynamics of the respective molecular species such as mRNA ( $r_I$ ,  $r_X$ ), monomeric protein ( $I$  or  $X$ ), and dimeric proteins ( $X_2$ ,  $XI$ ), where  $X$  stands for the activator  $A$  or repressor  $R$ , respectively. The regulatory homodimer  $X_2$  associates with  $G_0$  at a rate  $\alpha$  to form  $G_1$ , which disso-

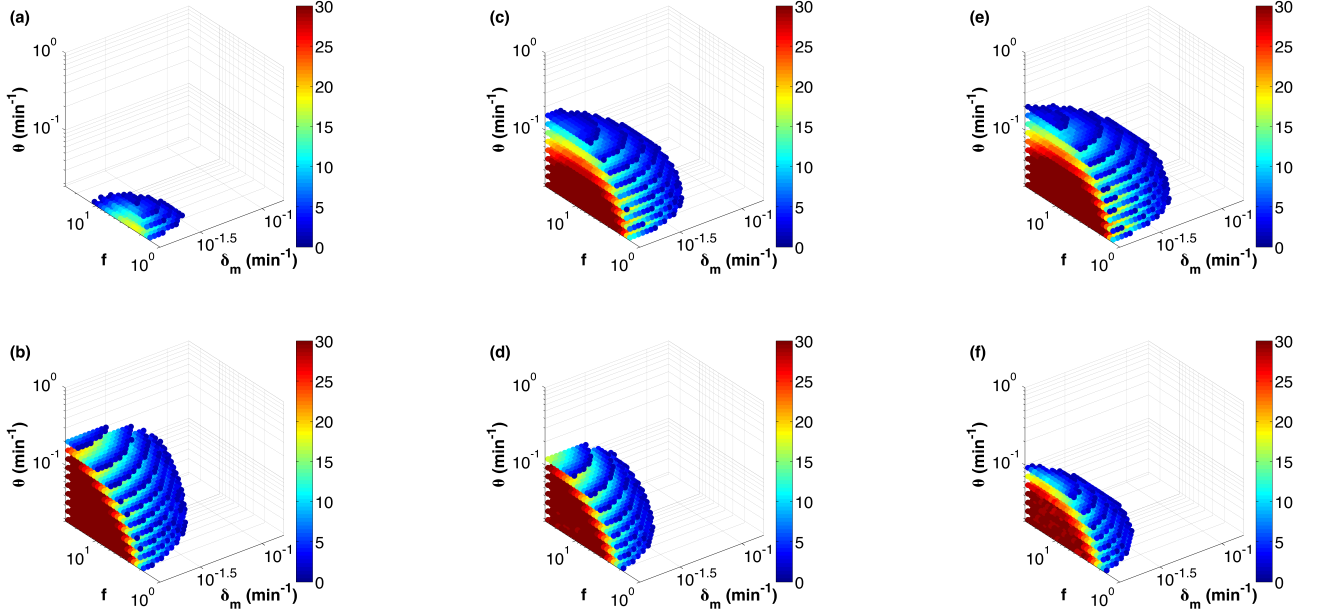


FIG. 3. (Color online) Parameter space of oscillatory solutions on a logarithmic scale for RTC (top) and ATC (bottom) with increasing DNA binding sites. The colormap shows the number of  $\rho_f$  values that exhibited oscillations for each combination of  $f$ ,  $\delta_m$ , and  $\theta$ . (a) and (b), single DNA binding site for RTC and ATC, (c) and (d) three independent binding sites for RTC and ATC, (e) and (f), three synergistic binding sites for RTC and ATC, where activation/repression strength is  $f^2$  when more than one activator/repressor is bound.

ciates at the rate  $\theta$ . The  $r_I$  and  $r_X$  are the inhibitor and activator/repressor mRNAs. For the ATC, the activator mRNA [ $r_X$ ] is transcribed constitutively at the rate  $\rho_0$ , where as the inhibitor mRNA is transcribed at rates  $\rho_f$  and  $\rho_b$  from free and bound DNA, respectively (Eqs. 2a,b). In contrast, for the RTC, the repressor mRNA is transcribed at rates  $\rho_f$  and  $\rho_b$  (Eqs. 3a,b) while inhibitor mRNA  $r_I$  is constitutively transcribed at the rate  $\rho_0$ . We assume that all mRNA species are degraded at the same rate  $\delta_m$  and translated into proteins with the same rate  $\beta$ . The activator/repressor  $X$  protein dimerizes into active homodimer  $X_2$  and forms inactive heterodimer  $XI$  with the inhibitor protein  $I$  at the same rate  $\gamma$ . The homodimer and heterodimer dissociation rates are  $\epsilon_1$  and  $\epsilon_2$ , respectively. We assume that all protein species are stable and diluted by cell growth at rate  $\delta_p$ .

## B. DNA unbinding kinetics influence oscillation

Our parameters were restricted to physiological values from yeast (see Table I). Most parameters were kept fixed, but we varied four key parameters. The first parameter was the mRNA production rate ( $\rho_f$ ) of free, unbound promoter because a desired expression level can easily be selected from existing promoter libraries [40]. Second, we varied the activation/repression strength ( $f$ ), which is the ratio of the larger  $\rho$  divided by the smaller  $\rho$ . Thus,  $f = \rho_b/\rho_f$  for the ATC and  $f = \rho_f/\rho_b$  for the

RTC. The ratio  $f$  can be tuned by appropriate choice of activation or repression domains fused to our bZIP transcription factor [41–43]. The third parameter was the mRNA degradation rate ( $\delta_m$ ), which is known to set the time scale of the ATC oscillator [19]. Last, we varied the DNA unbinding rate ( $\theta$ ) because it is our point of focus and this parameter can vary between different transcription factors. The DNA dissociation constant ( $K_d$ ) fixes the DNA binding rate  $\alpha = \frac{\theta}{K_d}$ ; see Appendix for details.

We divided the physiological range of each variable parameter into 30 values (on a logarithmic scale) and evaluated the long-term dynamics of a total of  $(30)^4$  parameter sets per circuit. We solved the ODEs over time for each set of  $(\rho_f, f, \delta_m, \theta)$ . A solution was classified as oscillatory if the trough of activator or repressor homodimer concentration was below the  $K_d$  of DNA-binding and if the peak was above  $2K_d$ ; see Appendix for justification. We noticed that  $\rho_f$  had the smallest effect on the number of oscillatory solutions and, thus, we plot the marginal frequency distribution of oscillatory solutions over  $f$ ,  $\delta_m$ , and  $\theta$  in Fig. 3. We see that strong activators (large  $f$  for the ATC), stable mRNAs (small  $\delta_m$ ), and slow DNA unbinding rates (small  $\theta$ ) generally favor oscillation. The last two parameters dictate the timescale of the delay in the negative feedback loop. Increased delay supports oscillation and, thus, the largest number of oscillatory solutions occur at the smallest  $\theta$  and  $\delta_m$  for both RTC (Fig. 3a) and ATC (Fig. 3b). The parameter space of stable oscillations is larger in ATC relative to RTC for a single

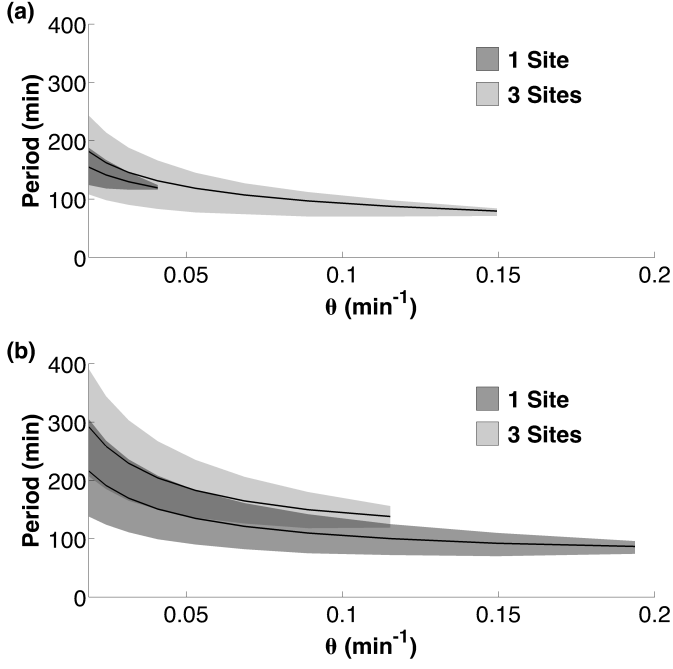


FIG. 4. The DNA unbinding rate  $\theta$  sets the period of the oscillations for RTC (a) and ATC (b) at slow unbinding rates. The mean period of oscillatory solutions for a given  $\theta$  is shown (solid black line) with the shaded area representing the range of periods.

binding site because of the additional step and delay in the negative feedback loop: negative feedback through the activator in the ATC is indirect (i.e. activator regulates the expression of inhibitor, which then inhibits its activity), whereas the self-repressor in the RTC is direct (i.e. repressor regulates its own expression).

The period of oscillation  $\tau$  should be set by the timescale of the slowest parameters in the delay. The negative feedback in our circuits is dominated by DNA unbinding rate  $\theta$  and mRNA degradation rate  $\delta_m$  [19]. This relationship can be seen in Figure 4 where the DNA unbinding rate sets the oscillation period at low  $\theta$ . An increase in  $\theta$  leads to mRNA degradation rate ( $\delta_m$ ) becoming the slower timescale at which point  $\tau$  becomes flatter and less dependent on  $\theta$ . Eventually, a bifurcation occurs at a critical, maximum value of  $\theta_{\max}$  which leads to loss of the stable limit cycle. A similar relationship exists for the mRNA degradation rate  $\delta_m$ ; see Figure S2.

### C. Multiple DNA binding sites affect ATC and RTC oscillators differently

This role of DNA unbinding rate in generating delays led us to hypothesize that multiple DNA binding sites should increase the parameter space of oscillations and lengthen the period of the oscillators. We reasoned

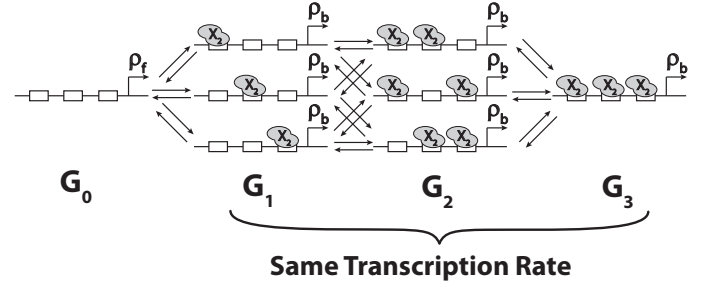


FIG. 5. Transitions between promoter states for multiple DNA binding sites ( $n=3$ ).  $G_i$  denotes the set of promoter states with  $i$  out of total  $n$  binding sites occupied by activator ( $X=A$ ) or repressor ( $X=R$ ) dimers. There are  $n-i$  ways of switching from  $G_i$  to  $[G_{i+1}]$  via the binding of  $X_2$ , and there are  $i$  ways of switching from  $G_i$  to  $G_{i-1}$  by the unbinding of  $X_2$ . Our model conservatively assumes that the binding of  $X_2$  does not affect the binding or unbinding of the next transcription factor to an adjacent site (no cooperativity). We also assume that the transcription rate is equal to  $\rho_b$  for  $G_1, G_2, \dots, G_n$  promoter states.

that if the occupancy of *any* binding site by a transcription factor activates or represses transcription, then the effective unbinding rate ( $\theta_n$ ) from a state of saturated DNA binding to the unbound DNA state ( $G_0$ , where the transcription rate changes) should decrease with the increasing number of binding sites ( $n$ ). We can show that  $\theta_n = \theta/H_n$ , where  $H_n$  is the  $n$ -th harmonic number (see Supplement [44]).

The addition of multiple DNA binding sites to our model will modify Eqs. (1a-b, 1f) by increasing the number of promoter states that can be bound by  $X_2$ ; see Figure 5 and Supplement [44]. For three binding sites ( $n=3$ ), our new Eqs (1a-b) are:

$$\begin{aligned} \frac{d[G_0]}{dt} &= -3\alpha \cdot [G_0][X_2] + \theta[G_1] \\ \frac{d[G_1]}{dt} &= 3\alpha \cdot [G_0][X_2] - (\theta + 2\alpha \cdot [X_2])[G_1] + 2\theta \cdot [G_2] \\ \frac{d[G_2]}{dt} &= 2\alpha \cdot [G_1][X_2] - (2\theta + \alpha \cdot [X_2])[G_2] + 3\theta \cdot [G_3] \\ \frac{d[G_3]}{dt} &= \alpha \cdot [G_2][X_2] - 3\theta \cdot [G_3] \end{aligned} \quad (4)$$

where the total concentration of DNA  $[G_T] = [G_0] + [G_1] + \dots + [G_n]$  is fixed to  $1/(N_A \cdot V) = 1/24$  nM. For three binding sites ( $n=3$ ), the term  $-\alpha[G_0][X_2] + \theta[G_1]$  in Eq. (1f) is replaced with:

$$-\sum_{i=0}^3 (3-i)\alpha \cdot [G_i][X_2] + \sum_{i=0}^3 i \cdot \theta[G_i] \quad (5)$$

$G_i$  denotes the promoter states with  $i$  out of total  $n$  binding sites occupied by activator ( $X=A$ ) or repressor ( $X=R$ ) dimers. The factors in front of each term represents the amount of degeneracy of each state, i.e.  $[G_i]$  has

$i$  bound sites, thus  $i$  ways of switching to  $[G_{i-1}]$ . Therefore, we have the term  $i \cdot \theta [G_i]$ . At the same time,  $[G_i]$  has  $n - i$  vacant sites, so it has  $n - i$  ways of switching to the state  $[G_{i+1}]$ . Thus, we have the term  $(n - i) \alpha \cdot [G_i][X_2]$ .

The addition of two more independent DNA binding sites dramatically increased the oscillatory space of the RTC (Fig. 3c), while slightly decreasing the oscillatory space of the ATC (Fig. 3d). These opposite results arise from a compound effect. First, two extra binding sites decreased the effective unbinding rate for the promoter to be fully vacated by half ( $\theta/H_3 \approx \theta/2$ ). This decrease in effective  $\theta$  increased the delay and resulted in some improvement in oscillations for both RTC and ATC. This effect is best observed in the increased period of both oscillators (Fig. 4). The second, more dominant effect is the fundamental difference in how the promoter sensitivity changes with multiple, independent binding sites. It is well established that nonlinear promoter responses facilitate oscillation [28]. We use the logarithmic sensitivity ( $S$ ) to quantify the nonlinearity in the promoter response, where  $S = d\log P/d\log[X_2]$  [45].  $P$  is the synthesis rate of the promoter and  $[X_2]$  is the activator/repressor homodimer concentration that regulates the promoter. As shown previously [45, 46], an increase in the number of independent repressive binding sites will increase the magnitude of  $S$  and create an ultrasensitive promoter response, (i.e.  $|S| > 1$ , see Supplement [44]). However, increasing the number of independent activating binding sites cannot generate an ultrasensitive promoter response ( $|S| \leq 1$ ); see Discussion in [45]. In fact, the logarithmic sensitivity for activation actually decreased with the number of binding sites at our physiological concentrations (see Supplement [44]). This difference is the reason why the RTC and ATC oscillators exhibited fundamental differences to increased number of binding sites. Our work shows that synthetic repression-based oscillators are preferable designs because the RTC gets an effective boost in promoter ultrasensitivity simply by adding multiple, independent binding sites.

We also tested whether synergistic repression or activation might change our results. Synergistic activation or repression occurs when the states that have more than one binding site occupied (i.e.  $G_2$  and  $G_3$ ) are activated/repressed  $f^2$ -fold instead of  $f$ -fold because they can interact with RNA polymerase at several interfaces [45]. Although this synergy increased the activation or repression strength, it did not significantly change the oscillatory parameter space (Fig. 3e,f).

### III. STOCHASTIC SIMULATIONS

Deterministic simulations were useful for understanding how DNA unbinding rate and the number of binding sites affect the phase space and period of oscillation. However, they cannot provide insights into the loss of temporal coherence that arises from stochastic gene expression. To this end, we used the Gillespie algorithm

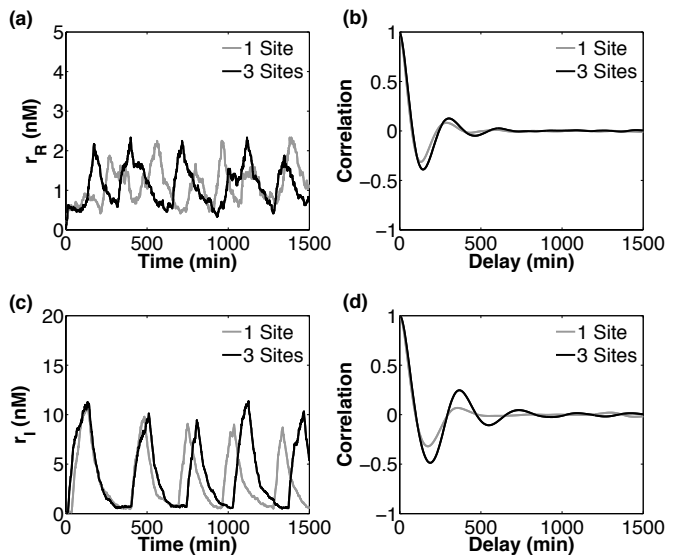


FIG. 6. Sample stochastic trajectories for one and three binding sites for RTC (a) and ATC (c), and their autocorrelation functions (b,d). The variable parameter values ( $\theta$ ,  $\delta_m$ ,  $\rho_f$ ,  $f$ ) were fixed to (0.02 min<sup>-1</sup>, 0.0159 min<sup>-1</sup>, 0.8928 min<sup>-1</sup>, 3.63) for the RTC and (0.02 min<sup>-1</sup>, 0.0186 min<sup>-1</sup>, 0.1781 min<sup>-1</sup>, 30) for the ATC. We chose parameters that produced oscillation over the largest range of DNA unbinding rates. The rest of the parameters are given in Table 1.

[47] to simulate stochastic chemical reaction kinetics and investigate how DNA binding/ unbinding dynamics and the addition of binding sites affect the temporal coherence of ATC and RTC oscillators.

For each ATC and RTC, we quantified temporal coherence by calculating the autocorrelation function of mRNA transcripts levels (repressor mRNA for the RTC and inhibitor mRNA for the ATC); see Fig. 6. In the absence of noise, an undamped oscillatory signal will have an undamped, periodic autocorrelation function. The presence of noise will stochastically perturb period and phase, such that the autocorrelation now exhibits dampening or loss of temporal coherence. We quantified the loss of coherence by measuring the rate of exponential decay ( $e^{-t/\tau_0}$ ) of the envelope of a periodic ( $\cos(2\pi t/\tau)$ ) autocorrelation function (see Appendix for details). Similar to other studies [4, 18], our metric for temporal coherence is the normalized autocorrelation function decay rate, which is the ratio of timescales  $\tau_0/\tau$ . A larger ratio indicates better temporal coherence. We varied the DNA unbinding rate ( $\theta$ ) and number of binding sites ( $n$ ) to understand the role of each feature in resisting molecular noise.

#### A. DNA Unbinding Rate

Our results show that ATC and RTC oscillators with smaller DNA unbinding rates exhibit better temporal co-

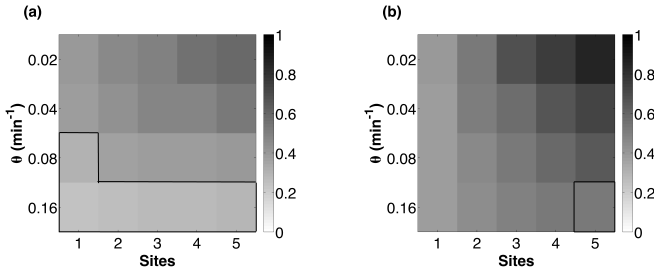


FIG. 7. The normalized autocorrelation function decay rate for the RTC (a) and ATC (b) for varying  $\theta$  and number of binding sites. All parameters, except  $\theta$ , are the same as in Fig. 6. Boxed, outlined regions are parameters past the bifurcation point ( $\theta_{\max}$ ) where deterministic oscillations are unsustainable and damped, yet exhibit stochastic excitable oscillations.

herence (Fig. 7). Lower  $\theta$  increases the temporal coherence of the oscillations because of the increased distance of the dynamical system from the bifurcation point ( $\theta_{\max}$ ); see Figure 8. Eventually there is another bifurcation at small  $\theta_{\min}$ , but these unbinding rates are unphysiological and do not affect our conclusions regarding biophysical ATC and RTC oscillators. Strikingly, some  $\theta > \theta_{\max}$ , which do not show deterministic oscillation, exhibit oscillation in the presence of noise. This phenomenon is consistent with coherence resonance [48] which has been observed in other excitable, genetic circuits near oscillatory bifurcation points [12, 24].

### B. Multiple DNA Binding Sites

Increasing the number of binding sites ( $n$ ) also increased the temporal coherence of ATC and RTC oscillators over all DNA unbinding rates (Fig. 7). To better understand this result, we must consider the effect of stochastic binding and unbinding of regulators on the variance of gene expression. In the phase of changing activator/repressor concentrations, the binding sites start being occupied or vacated. Each additional binding site introduces an additional DNA binding state. Because we treat the expression level of all bound DNA states as equivalent ( $\rho_b$ ), the spontaneous binding and unbinding events that occur between states that have at least one binding site occupied have no effect on transcription; see Fig. 5. These “protected” states act as a buffering mechanism to mitigate the effects of binary noise on temporal coherence.

## IV. DISCUSSION

We analyzed the properties of two titration based genetic oscillators, the activator-titration circuit (ATC) and the repressor-titration circuit (RTC). The focus of our study was to understand how the number of DNA

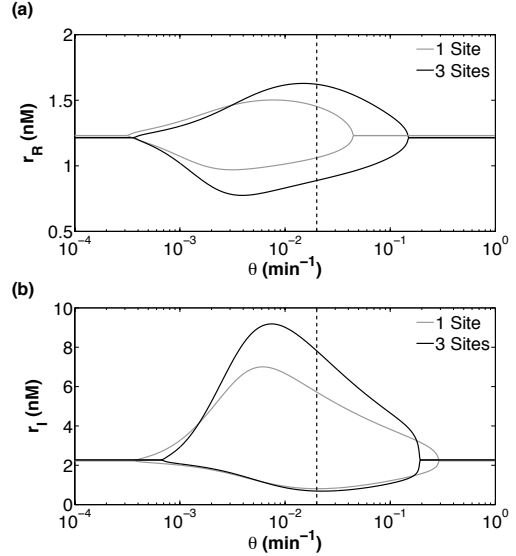


FIG. 8. Bifurcation diagram of the RTC (a) and ATC (b) oscillators as a function of DNA unbinding rate ( $\theta$ ). All parameters, except  $\theta$ , are the same as in Fig. 6. There are two bifurcation points ( $\theta_{\max}$ ,  $\theta_{\min}$ ) and the amplitude of mRNA oscillation is shown by the upper and lower branches. Physiological values of  $\theta$  are to the right of the dashed vertical line.

binding sites and slow unbinding kinetics in promoters mitigate or exacerbate the binary gene regulation noise. First, we showed that multiple DNA binding sites and slow unbinding kinetics were important for providing the necessary delay in the negative feedback loop for oscillatory solutions. The role of slow DNA binding/unbinding in providing delay for oscillations is consistent with prior work on a small negative feedback oscillator [9]. Second, we used stochastic simulation to show that slower DNA unbinding rates exhibited better temporal coherence, a result which appears at odds with previous work on circadian clocks and NF- $\kappa$ B oscillators [3, 10, 12] and which is more in line with the results obtained for a small negative feedback oscillator model [9]. This previous work showed that slower DNA unbinding kinetics negatively affected the temporal coherence for two reasons. First, slow DNA unbinding increased the stochasticity of gene expression due to imprecise concentration sampling, which decreased the temporal coherence of oscillations [3, 10]. Second, slower DNA unbinding ( $\theta$ ) pushed the dynamical system towards  $\theta_{\min}$  bifurcation point, which made it less robust to noise [12]. These results are different from ours because the delays in the circadian clock and NF- $\kappa$ B models rely on slow intermediate steps (e.g. phosphorylation and/or nuclear transport) in the negative feedback loop. Unlike our titration-based oscillators in Fig. 8, these models do not have  $\theta_{\max}$  and still oscillate at infinitely fast unbinding rates where the promoter dynamics are in steady-state.

We observed the opposite effect for our titration-based

oscillators because physiological  $\theta$  overlaps the  $\theta_{\max}$  bifurcation point for ATC/RTC. Thus, lowering  $\theta$  always increases the robustness in ATC/RTC because the dynamical system is moving away from  $\theta_{\max}$  and deeper into oscillatory parameter space. This phenomenon likely explains the similar results presented in [9]. The influence of DNA unbinding rate on temporal coherence depends on the structure of the underlying bifurcation diagram of each oscillator as a function of  $\theta$ . Changes in topology, mechanism, and parameters can change the bifurcation diagram and, thus, the influence of DNA unbinding rate on temporal coherence of oscillation may also change.

Last, we demonstrate that multiple independent binding sites consistently increased the temporal coherence of oscillations by alleviating the binary noise resulting from binary gene states. Our results agree with previous work, which showed that multiple, cooperative DNA binding sites increased the coherence of circadian clocks [18]. However, in contrast to our results, the temporal coherence of circadian clocks peaked at 3 binding sites and then decreased with additional sites. The difference likely arises from our slower DNA binding/unbinding rates, where the ATC and RTC oscillators spend significant time in protected states that are buffered against molecular noise. In contrast, the circadian clock model spends very little time in the intermediate protected states between fully free or fully bound promoters and, therefore, the increased coherence is only due to cooperativity [18]. The idea of buffering to reduce noise in gene circuits has been discussed in the context of decoy binding sites [49]. However, this requires fast DNA binding/unbinding, whereas buffering through promoter states requires slow DNA binding/unbinding. We note that increased temporal coherence due to protected states is a stochastic effect because the addition of binding sites consistently increased the coherence of ATC oscillators, despite occasionally pushing it past the bifurcation point at  $\theta_{\max}$  (Fig. 6b).

## Appendix A: Parameter Values

To constrain the physiological parameters of our models, we used data from large-scale studies of the yeast transcriptome and proteome; see Table I. These data provide typical ranges and values for our parameters. First, we converted numbers of molecules into nanomolar (nM) concentrations using the cell volume  $V = 40$  fL for haploid yeast. For the ATC, we assumed that the basal mRNA transcription would be low. Thus,  $\rho_f$  for the ATC was constrained to values from the bottom 5th percentile to the median of all mRNA synthesis rates [50]. Similarly,  $\rho_f$  for the RTC was constrained to values from the median to top 95th percentile. In the case of the ATC, the constraint  $\rho_f < \rho_0 < \rho_b$  ensured that the inhibitor can completely titrate the constitutively-expressed activator when the inhibitor is maximally produced at  $\rho_b$ , but not when it is expressed at the basal rate  $\rho_f$ . Similarly,

for the RTC, the constraint  $\rho_b < \rho_0 < \rho_f$  ensures that constitutively-expressed inhibitor can completely titrate the repressor when the repressor is produced at the repressed rate  $\rho_b$ , but not  $\rho_f$ . We set  $\rho_0 = \sqrt{\rho_f \rho_b}$  to satisfy both conditions. mRNA degradation rate ranged from the bottom 5th percentile to top 95th percentile values for all genes [50]. To obtain a rough approximation for the translation rates, we assumed a constitutive gene expression model for all genes:

$$\frac{d[r]}{dt} = \rho - \delta_m[r] \quad (A1)$$

$$\frac{d[P]}{dt} = \beta[r] - \delta_p[P] \quad (A2)$$

At steady state,  $\beta = \frac{[P]\delta_p\delta_m}{\rho}$ . Protein concentrations and degradation rates were taken from [51, 52]. We calculated  $\beta$  for all genes and used the median value in our model. We also assumed that our activators, repressors, and inhibitors are not actively degraded and are diluted by growth. Thus,  $\delta_p = \ln(2)/T$ , where  $T = 90$  mins is the duration of the yeast cell cycle. The proteins in our models were based on a mammalian transcription factor basic leucine zipper (bZIP) protein C/EBP $\alpha$  and its dominant-negative inhibitor (3HF) [37]. We used previously measured rates for protein-protein interaction kinetics [37]. Since we did not know the DNA unbinding rate for C/EBP $\alpha$ , we considered the range for the known DNA unbinding rates for other bZIP proteins [13–16]. The thermodynamic dissociation constant ( $K_d$ ) of C/EBP $\alpha$  to its specific DNA binding site is known [39]. We set the DNA association rate to  $\alpha = \theta/K_d$ . Finally, we varied the activation/repression strength  $f$  from 1 to 30, to consider both strong and weak activation/repression.

## Appendix B: Methods

We scanned the parameter space for oscillations by running simulations on MATLAB (Mathworks) using ode15s for 2000 min and recording the minima and maxima of the activator/repressor homodimer during the last 1000 min. We imposed the following restrictions: 1) the last minimum should be below  $K_d$  so that DNA-binding is not saturated, 2) the last maximum should be greater than  $2K_d$  so that the change in transcription is noticeably altered. While this restriction slightly underestimates the number oscillatory solutions, it ensures that a synthetic version of these circuits would produce detectable oscillations. We verified that our definition gave similar results to a less stringent criterion for oscillation.

We used the direct Gillespie method to perform the stochastic simulations [53]. We ran the simulations for  $10^6$  min and recorded the concentration of the regulated mRNA (inhibitor for the ATC and the repressor for the RTC). We then normalized the concentration such that the average would be zero and evaluated

TABLE I. Parameter values

Parameter	Min	Max	Reference
$\theta(\text{min}^{-1})$	0.0188	34.5	[13–16]
ATC $\rho_f(\text{min}^{-1})$	0.0509	0.1781	[50]
RTC $\rho_f(\text{min}^{-1})$	0.1781	0.8928	[50]
$\delta_m(\text{min}^{-1})$	0.0159	0.1516	[50]
$f$	1	30	
ATC $\rho_b(\text{min}^{-1})$	$f \cdot \rho_f$		
RTC $\rho_b(\text{min}^{-1})$	$\rho_f/f$		
$\alpha(\text{nM}^{-1} \text{ min}^{-1})$	$\theta/3.344 \text{ nM}$		[39]
$\rho_0(\text{min}^{-1})$	$\sqrt{\rho_f \rho_b}$		
$\beta(\text{min}^{-1})$	14.1		[50–52]
$\delta_p(\text{min}^{-1})$	0.0077		
$\gamma(\text{nM min}^{-1})$	0.6		[37]
$\epsilon_1(\text{min}^{-1})$	6		[37]
$\epsilon_2(\text{min}^{-1})$	0.024		[37]
$V(\text{fL})$	40		[27]

the autocorrelation function. We then fit the function  $C(t) = e^{-t/\tau_0} \cdot \cos(2\pi t/\tau)$  to the first 1500 min of the autocorrelation function to measure the decay constant  $\tau_0$  and period  $\tau$ . The ratio  $\tau_0/\tau$  describes how rapidly the envelope of autocorrelation function decays per oscillation period.

## ACKNOWLEDGMENTS

We thank Joshua Socolar for helpful comments. This work was funded by an NIH Director’s New Innovator Award (DP2 OD008654-01) and Burroughs Wellcome Fund CASI Award (BWF 1005769.01). An SBML version of the ATC and RTC oscillators can be downloaded from the BioModels Database (MODEL1512100000 and MODEL1512100001, respectively).

- [1] E. Schrödinger, *What is life? The physical aspect of the living cell* (Cambridge University Press, 1944).
- [2] D. Gonze, J. Halloy, and A. Goldbeter, *J. Biol. Phys.* **28**, 637 (2002).
- [3] D. B. Forger and C. S. Peskin, *Proc Natl Acad Sci USA* **102**, 321 (2005).
- [4] D. Gonze and A. Goldbeter, *Chaos* **16**, 026110 (2006).
- [5] I. Golding, J. Paulsson, S. M. Zawilski, and E. C. Cox, *Cell* **123**, 1025 (2005).
- [6] L. Cai, N. Friedman, and X. S. Xie, *Nature* **440**, 358 (2006).
- [7] J. E. M. Hornos, D. Schultz, G. C. P. Innocentini, J. Wang, A. M. Walczak, J. N. Onuchic, and P. G. Wolynes, *Phys. Rev. E* **72**, 051907 (2005).
- [8] A. M. Walczak, J. N. Onuchic, and P. G. Wolynes, *Proc Natl Acad Sci USA* **102**, 18926 (2005).
- [9] H. Feng, B. Han, and J. Wang, *Biophys. J* **102**, 1001 (2012).
- [10] D. A. Potoyan and P. G. Wolynes, *Proc Natl Acad Sci USA* **111**, 2391 (2014).
- [11] D. Labavić, H. Nagel, W. Janke, and H. Meyer-Ortmanns, *Phys. Rev. E* **87**, 062706 (2013).
- [12] D. Gonze, J. Halloy, and A. Goldbeter, *Physica A* **342**, 221 (2004).
- [13] H. Kwon, S. Park, S. Lee, D.-K. Lee, and C.-H. Yang, *Eur. J. Biochem.* **268**, 565 (2001).
- [14] M. Kyo, T. Yamamoto, H. Motohashi, T. Kamiya, T. Kuroita, T. Tanaka, J. D. Engel, B. Kawakami, and M. Yamamoto, *Genes Cells* **9**, 153 (2004).
- [15] Y. Okahata, K. Niikura, Y. Sugiura, M. Sawada, and T. Morii, *Biochemistry* **37**, 5666 (1998).
- [16] M. Geertz, D. Shore, and S. J. Maerkl, *Proc Natl Acad Sci USA* **109**, 16540 (2012).
- [17] P. Hammar, M. Walldén, D. Fange, F. Persson, Ö. Baltekin, G. Ullman, P. Leroy, and J. Elf, *Nat Genet* **46**, 405 (2014).
- [18] D. Gonze, J. Halloy, and A. Goldbeter, *Proc Natl Acad Sci USA* **99**, 673 (2002).
- [19] P. François and V. Hakim, *Phys. Rev. E* **72**, 031908 (2005).
- [20] J. Menet, K. Abruzzi, J. Desrochers, J. Rodriguez, and M. Rosbash, *Genes Dev* **24**, 358 (2010).
- [21] A. Hoffmann, A. Levchenko, M. L. Scott, and D. Baltimore, *Science* **298**, 1241 (2002).
- [22] D. E. Nelson, A. E. C. Ihekweaba, M. Elliott, J. R. Johnson, C. A. Gibney, B. E. Foreman, G. Nelson, V. See, C. A. Horton, D. G. Spiller, S. W. Edwards, H. P. McDowell, J. F. Unitt, E. Sullivan, R. Grimley, N. Benson, D. Broomhead, D. B. Kell, and M. R. H. White, *Science* **306**, 704 (2004).
- [23] N. Barkai and S. Leibler, *Nature* **403**, 267 (2000).
- [24] J. M. G. Vilar, H. Y. Kueh, N. Barkai, and S. Leibler, *Proc Natl Acad Sci USA* **99**, 5988 (2002).
- [25] S. Krishna, M. H. Jensen, and K. Sneppen, *Proc Natl Acad Sci USA* **103**, 10840 (2006).
- [26] J. K. Kim and D. B. Forger, *Mol Syst Biol* **8** (2012).
- [27] N. E. Buchler and M. Louis, *J Mol Biol* **384**, 1106 (2008).
- [28] B. Novak and J. J. Tyson, *Nat Rev Mol Cell Biol* **9**, 981 (2008).
- [29] M. B. Elowitz and S. Leibler, *Nature* **403**, 335 (2000).
- [30] M. R. Atkinson, M. A. Savageau, J. T. Myers, and A. J. Ninfa, *Cell* **113**, 597 (2003).
- [31] J. Stricker, S. Cookson, M. R. Bennett, W. H. Mather, L. S. Tsimring, and J. Hasty, *Nature* **456**, 516 (2008).
- [32] B. Novak and J. J. Tyson, *J Theor Biol* **165**, 101 (1993).
- [33] M. Nakajima, H. Ito, and T. Kondo, *FEBS Letters* **584**, 898 (2010).
- [34] Q. Yang and J. E. Ferrell, *Nature* **15**, 519 (2013).
- [35] W. W. Wong, T. Y. Tsai, and J. C. Liao, *Mol Syst Biol*

- 3**, 130 (2007).
- [36] O. Mondragón-Palomino, T. Danino, J. Selimkhanov, L. Tsimring, and J. Hasty, *Science* **333**, 1315 (2011).
  - [37] N. E. Buchler and F. R. Cross, *Mol Syst Biol* **5**, 272 (2009).
  - [38] D. Krylov, M. Olive, and C. Vinson, *EMBO J* **14**, 5329 (1995).
  - [39] Z. Cao, R. M. Umek, and S. L. McKnight, *Genes Dev.* **5**, 1538 (1991).
  - [40] L. Keren, O. Zackay, M. Lotan-Pompan, U. Barenholz, E. Dekel, V. Sasson, G. Aidelberg, A. Bren, D. Zeevi, A. Weinberger, U. Alon, R. Milo, and E. Segal, *Mol Syst Biol* **9** (2013).
  - [41] U. Baron, M. Gossen, and H. Bujard, *Nucleic Acids Res* **25**, 2723 (1997).
  - [42] G. Bellí, E. Garí, L. Piedrafita, M. Aldea, and E. Hertero, *Nucleic Acids Res* **26**, 942 (1998).
  - [43] P. Perez-Pinera, D. G. Ousterout, J. M. Brunger, A. M. Farin, K. A. Glass, F. Guilak, G. E. Crawford, A. J. Hartemink, and C. A. Gersbach, *Nat Methods* **10**, 239 (2013).
  - [44] See Supplemental Material at URL for the derivation of promoter sensitivity, unbinding from multiple sites and additional figures.
  - [45] L. Bintu, N. E. Buchler, H. G. Garcia, U. Gerland, T. Hwa, J. Kondev, T. Kuhlman, and R. Phillips, *Curr Opin Genet Dev* **15**, 125 (2005).
  - [46] I. M. Lengyel, D. Soroldoni, A. C. Oates, and L. G. Morelli, *Papers in Physics* **6** (2014).
  - [47] D. Gillespie, *J. Phys. Chem.* **81**, 2340 (1977).
  - [48] A. S. Pikovsky and J. Kurths, *Phys. Rev. Lett.* **78**, 775 (1997).
  - [49] A. Burger, A. M. Walczak, and P. G. Wolynes, *Phys. Rev. E* **86**, 041920 (2012).
  - [50] C. Miller, B. Schwalb, K. Maier, D. Schulz, S. Dümcke, B. Zacher, A. Mayer, J. Sydow, L. Marcinowski, L. Dölken, D. E. Martin, A. Tresch, and P. Cramer, *Mol Syst Biol* **7**, 458 (2011).
  - [51] S. Ghaemmaghami, W.-K. Huh, K. Bower, R. W. Howson, A. Belle, N. Dephoure, E. K. O'Shea, and J. S. Weissman, *Nature* **425**, 737 (2003).
  - [52] A. Belle, A. Tanay, L. Bitincka, R. Shamir, and E. K. O'Shea, *Proc Natl Acad Sci USA* **103**, 13004 (2006).
  - [53] S. Hoops, S. Sahle, R. Gauges, C. Lee, J. Pahle, N. Simus, M. Singhal, L. Xu, P. Mendes, and U. Kummer, *Bioinformatics* **22**, 3067 (2006).

## Supplementary Material

Sargis Karapetyan<sup>1,2</sup> and Nicolas E. Buchler<sup>1,2,3</sup>

<sup>1</sup>*Department of Physics, Duke University, Durham, NC 27708*

<sup>2</sup>*Center for Genomic & Computational Biology, Durham, NC 27710*

<sup>3</sup>*Department of Biology, Duke University, Durham, NC 27708*

## I. PROMOTER WITH MULTIPLE BINDING SITES

We first derive the chemical kinetic equations for 2 binding sites and then generalize to  $n$  binding sites [1]. Similar to previous work [2], we calculate the promoter sensitivity of activators and repressors in the limit of thermodynamic equilibrium.

### A. Promoter with 2 equal binding sites

We first begin with an explicit derivation that includes each binding state combination:

$$\frac{d[G_{00}]}{dt} = -\alpha \cdot [G_{00}][X_2] + \theta \cdot [G_{10}] - \alpha \cdot [G_{00}][X_2] + \theta \cdot [G_{01}] \quad (1)$$

$$\frac{d[G_{01}]}{dt} = \alpha \cdot [G_{00}][X_2] - \theta \cdot [G_{01}] - \alpha \cdot [G_{01}][X_2] + \theta \cdot [G_{11}] \quad (2)$$

$$\frac{d[G_{10}]}{dt} = \alpha \cdot [G_{00}][X_2] - \theta \cdot [G_{10}] - \alpha \cdot [G_{10}][X_2] + \theta \cdot [G_{11}] \quad (3)$$

$$\frac{d[G_{11}]}{dt} = \alpha \cdot [G_{10}][X_2] - \theta \cdot [G_{11}] + \alpha \cdot [G_{01}][X_2] - \theta \cdot [G_{11}] \quad (4)$$

where  $[G_T] = [G_{00}] + [G_{01}] + [G_{10}] + [G_{11}]$  and  $[X_2]$  is the homodimer transcription factor concentration. We rewrite these equations in a compact form:

$$\frac{d[G_0]}{dt} = -2\alpha \cdot [G_0][X_2] + \theta[G_1] \quad (5)$$

$$\frac{d[G_1]}{dt} = 2\alpha \cdot [G_0][X_2] - \theta[G_1] - \alpha[G_1][X_2] + 2\theta[G_2] \quad (6)$$

$$\frac{d[G_2]}{dt} = \alpha \cdot [G_1][X_2] - 2\theta[G_2] \quad (7)$$

where  $[G_0] = [G_{00}]$ ,  $[G_1] = [G_{01}] + [G_{10}]$ , and  $[G_2] = [G_{11}]$ . This simplification is valid when all binding sites have equivalent kinetics and the regulator  $X_2$  binds independently to each site.

#### 1. Promoter synthesis rate at equilibrium

At equilibrium, Eqs. (5-7) are equal to 0. Thus,

$$2[G_0][X_2] = K_d \cdot [G_1] \quad (8)$$

$$(K_d + [X_2])[G_1] = 2[G_0][X_2] + 2K_d \cdot [G_2] \quad (9)$$

$$[G_1] \cdot [X_2] = 2K_d \cdot [G_2] \quad (10)$$

where  $K_d = \theta/\alpha$ . Solving these equations with constraint  $[G_T] = [G_0] + [G_1] + [G_2]$ :

$$[G_0] = [G_T] \cdot \frac{1}{(1 + \frac{[X_2]}{K_d})^2} \quad (11)$$

$$[G_1] = [G_T] \cdot \frac{2 \cdot (\frac{[X_2]}{K_d})}{(1 + \frac{[X_2]}{K_d})^2} \quad (12)$$

$$[G_2] = [G_T] \cdot \frac{(\frac{[X_2]}{K_d})^2}{(1 + \frac{[X_2]}{K_d})^2} \quad (13)$$

The promoter synthesis rate  $P_2$  where any bound state has the same gene expression ( $\rho_b$ ) and the unbound state has gene expression ( $\rho_f$ ) is given by:

$$P_2(X_2) = [G_T] \cdot \left[ \frac{\rho_b [2 \cdot X_2 + (X_2)^2] + \rho_f}{(1 + X_2)^2} \right] = [G_T] \cdot \left[ \rho_b + \frac{(\rho_f - \rho_b)}{(1 + X_2)^2} \right] \quad (14)$$

where  $X_2 = \frac{[X_2]}{K_d}$ .

## B. Promoter with n equal binding sites

By generalizing our previous derivation for an arbitrary number of binding sites, we get  $n + 1$  differential equations, where  $n$  is the total number of binding sites and the index  $i$  spans  $1 \leq i \leq n - 1$ .

$$\frac{d[G_0]}{dt} = -n\alpha \cdot [G_0][X_2] + \theta[G_1] \quad (15)$$

$\vdots$

$$\frac{d[G_i]}{dt} = (n - i + 1)\alpha \cdot [G_{i-1}][X_2] - (i \cdot \theta + (n - i)\alpha \cdot [X_2])[G_i] + (i + 1)\theta \cdot [G_{i+1}] \quad (16)$$

$\vdots$

$$\frac{d[G_n]}{dt} = \alpha \cdot [G_{n-1}][X_2] - n\theta \cdot [G_n] \quad (17)$$

$G_i$  denotes the promoter states with  $i$  out of total  $n$  binding sites occupied by activator (X=A) or repressor (X=R) dimers. The factors in front of each term represents the amount of degeneracy of each state, i.e  $[G_i]$  has  $i$  bound sites, thus  $i$  ways of switching to  $[G_{i-1}]$ . Therefore, we have the term  $i \cdot \theta[G_i]$ . At the same time,  $[G_i]$  has  $n - i$  vacant sites, so it has  $n - i$  ways of switching to the state  $[G_{i+1}]$ . Thus, we have the term  $(n - i)\alpha \cdot [X_2][G_i]$ . Note that our model assumes that the binding of a transcription factor does not affect the binding or unbinding of the next transcription factor to an adjacent site (no cooperativity). We also assume that transcription is fully activated/repressed for any bound state of the promoter, i.e. transcription is equal to  $\rho_b$  for  $G_1, G_2, \dots, G_n$ . Although not shown, the ODE for the rate of change in dimer concentration Eq. (1f) in the main text is also modified to reflect binding and unbinding from each state  $G_i$ .

### 1. Promoter synthesis rate at equilibrium

Setting Equations (15-17) equal to zero and solving with the constraint  $[G_T] = [G_0] + [G_1] + \dots + [G_n]$ :

$$[G_0] = [G_T] \cdot \frac{1}{(1 + \frac{[X_2]}{K_d})^N} \quad (18)$$

$\vdots$

$$[G_i] = [G_T] \cdot \frac{\frac{N!}{i!(N-i)!} \cdot (\frac{[X_2]}{K_d})^i}{(1 + \frac{[X_2]}{K_d})^N} \quad (19)$$

$\vdots$

$$[G_N] = [G_T] \cdot \frac{(\frac{[X_2]}{K_d})^N}{(1 + \frac{[X_2]}{K_d})^N} \quad (20)$$

The promoter synthesis rate  $P_n$  is thus given by:

$$P_n(X_2) = [G_T] \cdot \left[ \rho_b + \frac{(\rho_f - \rho_b)}{(1 + X_2)^n} \right] \quad (21)$$

where  $X_2 = \frac{[X_2]}{K_d}$ .

### C. Logarithmic sensitivity analysis

We compute the logarithmic sensitivity of the promoter:  $S = \frac{d \log P}{d \log X_2} = \frac{X_2}{P(X_2)} \cdot \frac{dP}{dX_2}$ :

$$S(X_2) = \frac{n(\rho_b - \rho_f)X_2}{(1 + X_2) \cdot (\rho_f + \rho_b[(1 + X_2)^n - 1])} \quad (22)$$

#### 1. Activation

We consider the simplified case of ideal activation, where  $\rho_f = 0$ . Thus,

$$S(X_2) = \frac{nX_2}{(1 + X_2) \cdot [(1 + X_2)^n - 1]} \quad (23)$$

$S$  is a monotonically decreasing function of  $X_2$  with boundaries  $S(0) = 1$  and  $S(\infty) = 0$ . Thus, activation is never ultrasensitive (i.e.  $|S| \leq 1$  for any value of  $X_2$ ,  $n$ , or  $\rho_b$ ). Additionally,  $|S|$  is also a monotonically decreasing function of  $n$  for all  $X_2 > 0$ ; see Figure S1. The boundaries are at  $|S(0)| = \frac{X_2}{(1+X_2) \cdot \ln(1+X_2)}$  and  $|S(\infty)| = 0$ . This explains why the ATC oscillator phase space decreases with the addition of multiple DNA binding sites.

#### 2. Repression

We consider the case of ideal repression where  $\rho_b = 0$ . Thus,

$$S(X_2) = \frac{-nX_2}{(1 + X_2)} \quad (24)$$

$S$  is a monotonically decreasing function of  $R$  with boundaries  $S(0) = 0$  and  $S(\infty) = -n$ . Promoter repression is ultrasensitive (i.e.  $|S| > 1$ ) for  $X_2 > \frac{1}{n-1}$  and  $n > 1$ ; see Figure S1.  $|S|$  is a monotonically increasing function of  $n$  for all  $X_2 > 0$ . The boundaries are at  $|S(0)| = 0$  and  $|S(\infty)| = \infty$ . Thus, the RTC oscillator phase space increases with the addition of multiple DNA binding site.

## II. KINETICS OF COMPLETE UNBINDING FROM MULTIPLE SITES

The probability of unbinding for a single binding site is given by a Poisson distribution:

$$p(t) = \theta e^{-\theta t} \quad (25)$$

where  $\theta$  is the unbinding rate. The average unbinding time for a single site is given by  $\langle \tau \rangle = \int_0^\infty t \cdot p(t) dt$  and is equal to  $\frac{1}{\theta}$ . Consider the case where all  $n$  binding sites are filled and where the concentration of regulator abruptly changes to 0 (such that no rebinding occurs). We calculate the probability distribution of time for *complete* unbinding from all  $n$  binding sites. The probability that the slowest unbinding event is  $\tau$  and the other  $n - 1$  events are less than  $\tau$  is:

$$\mathcal{P}(\tau|n, \theta) = \left[ \int_0^\tau p(t) dt \right]^{n-1} \cdot p(\tau) \quad (26)$$

$$\mathcal{P}(\tau|n, \theta) = [1 - e^{-\theta\tau}]^{n-1} \cdot \theta e^{-\theta\tau} \quad (27)$$

When we normalize the distribution ( $\int_0^\infty \mathcal{P}(\tau|n, \theta) d\tau = 1$ ):

$$\mathcal{P}(\tau|n, \theta) = n [1 - e^{-\theta\tau}]^{n-1} \cdot \theta e^{-\theta\tau} \quad (28)$$

The average  $\langle \tau \rangle$  can be calculated by  $\int_0^\infty \tau \cdot \mathcal{P}(\tau) d\tau$ :

$$\langle \tau \rangle = \frac{H_n}{\theta} = \frac{1}{\theta_n} \quad (29)$$

where  $H_n = 1 + \frac{1}{2} + \frac{1}{3} + \dots + \frac{1}{n}$  (Harmonic number) and  $\theta_n$  is the effective DNA unbinding rate.

### III. SUPPORTING FIGURES

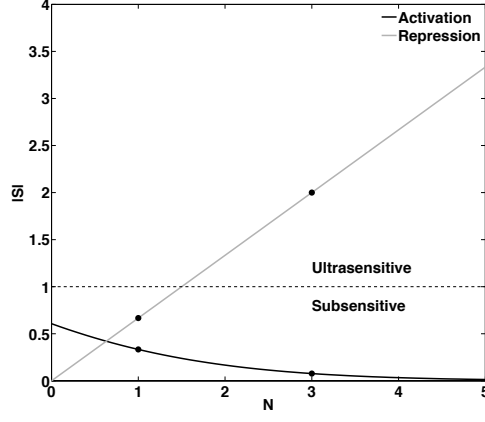


FIG. S1. Multiple binding sites affect activation- and repression-based promoters differently. The absolute value of logarithmic sensitivity  $S$  is plotted as a function of number of binding sites  $N$ , with  $X_2 = 2$ . The points of 1 and 3 binding sites considered in this study are marked with circles.

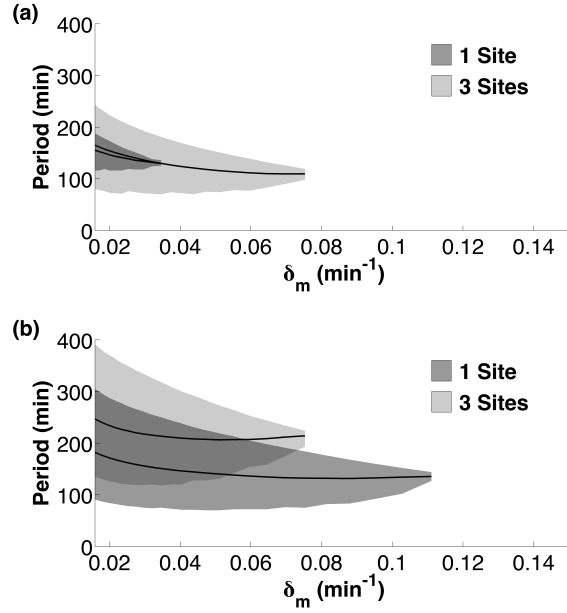


FIG. S2. The mRNA degradation rate  $\delta_m$  sets the period of the oscillations for RTC (a) and ATC (b) at slow mRNA degradation rates. The mean period of oscillatory solutions for a given  $\delta_m$  is shown (solid black line) with the shaded area representing the range of periods.

- 
- [1] I. M. Lengyel, D. Soroldoni, A. C. Oates, and L. G. Morelli, *Papers in Physics* **6** (2014).
- [2] L. Bintu, N. E. Buchler, H. G. Garcia, U. Gerland, T. Hwa, J. Kondev, T. Kuhlman, and R. Phillips, *Curr Opin Genet Dev* **15**, 125 (2005).